Practical Considerations for Computing Dimensional Spectra from Gridded Data

DALE DURRAN, JONATHAN A. WEYN, AND MAXIMO Q. MENCHACA

Department of Atmospheric Sciences, University of Washington, Seattle, Washington

(Manuscript received 6 March 2017, in final form 6 July 2017)

ABSTRACT

Spectra are often computed from gridded data to determine the horizontal-scale dependence of quantities such as kinetic energy, vertical velocity, or perturbation potential temperature. This paper discusses several important considerations for the practical computation of such spectra. To ensure that the sum of the spectral energy densities in wavenumber space matches the sum of the energies in the physical domain (the discrete Parseval relation), the constant coefficient multiplying the spectral energy density must properly account for the way the discrete Fourier transform pair is normalized. The normalization factor appropriate of many older FORTRAN-based fast Fourier transforms (FFTs) differs from that in Matlab and Python's numpy.fft, and as a consequence, the correct scaling factor for the kinetic energy (KE) spectral density differs between one-dimensional FFTs computed using these two approaches by a factor equal to the square of the number of physical grid points. A common algorithm used to compute two-dimensional spectra as a function of the total-wavenumber magnitude sums the contributions from all pairs of x- and y-component wavenumbers whose vector magnitude lies with a series of bins. This approach introduces systematic short-wavelength noise, which can be largely eliminated though a simple multiplicative correction. One- and two-dimensional spectra will differ by a constant if computed for flows in which the KE spectral density decreases as a function of the wavenumber to some negative power. This constant is evaluated and the extension of theoretical results to numerically computed FFTs is examined.

1. Introduction

When computing spectra from observed or model data, the main focus is often on the slope of the spectrum as a function of wavenumber on a log–log plot. Nevertheless, if such spectra are to be quantitatively compared with those obtained in other studies (as in, e.g., Skamarock 2004; Hamilton et al. 2008), it is important to be able to correctly compute the magnitude of the energy spectral density. The goal of this article is to facilitate such comparisons.

The discrete Fourier transform (DFT) of a vector $\mathbf{u}$ of length N is often defined as

$$\hat{u}_m = n_1 \sum_{j=1}^{N} u_j \omega_N^{(m-1)(j-1)}, \tag{1}$$

together with the inverse transform:

$$u_j = n_2 \sum_{m=1}^{N} \hat{u}_m \omega_N^{-(m-1)(j-1)}, \tag{2}$$

where $n_1 n_2 = 1/N$ and, following the typical "roots of unity" notation, $\omega_N = e^{-2\pi i/N}$ (Durran 2010). Neither the choice of the signs in the exponents nor the distribution of the normalization factors n_1 and n_2 between (1) and (2) are standardized. The only requirement is that the product of the normalization factors equals $1/N$ and that the exponents have opposite signs. Many classical treatments of the DFT follow the convention $(n_1, n_2) = (1/N, 1)$ (Cooley et al. 1970; Durran 2010), but the DFT in Matlab and Python (specifically Matlab's FFT–IFFT pair and the default option in Python's numpy.fft module) follow the opposite convention $(n_1, n_2) = (1, 1/N)$. The choice of (n_1, n_2) impacts the discrete Parseval relation and as a consequence, the dimensional coefficients that should appear in the computation of energy spectral densities. One purpose of this article is to clarify the factors that should appear in dimensional atmospheric spectra, for example to compare commonly computed horizontal kinetic energy (KE) spectra in gridded models with observations (Nastrom and Gage 1985; Cho et al. 1999). The correct dimensional scaling for one-dimensional spectra is discussed in

Corresponding author: Dale Durran, drdee@uw.edu

DOI: 10.1175/MWR-D-17-0056.1

section 2, while that for two-dimensional spectra is presented in section 3.

The second purpose of this article is to highlight a simple technique for reducing systematic noise in the computation of two-dimensional spectra. Two-dimensional spectra are typically evaluated as a function of total wavenumber $k_h = (k_x^2 + k_y^2)^{1/2}$, where k_x and k_y are the wavenumbers parallel to each coordinate axis, which we label as x and y. For continuous Fourier transforms, the KE spectral density at k_h is evaluated by integrating around a ring of radius k_h centered at the origin in the $k_x - k_y$ plane. The corresponding calculation for discrete data often follows the procedure detailed in Errico (1985) in which the integral around a ring in the $k_x - k_y$ plane is replaced by summing up the energies of all (k_x, k_y) pairs that lie with annular rings. This procedure introduces *systematic* noise, and as briefly noted in Tanguay et al. (1995), such noise can be easily eliminated through multiplication by a compensating factor, as will be discussed in section 4.

The final topic, investigated in section 5, is the difference in the magnitude of one-dimensional and two-dimensional KE spectra computed for the same flow. The theoretical discussion in Leith (1971) for isotropic horizontally nondivergent flow is first generalized; then we examine the influence of the numerical approximations that accompany the computation of discrete Fourier transforms. Finally we compare one-dimensional and two-dimensional KE spectra in a physically relevant divergent, anisotropic flow.

Throughout the following we assume the data are periodic. If the data are not periodic, they can be made periodic by removing the linear trend along lines parallel to each coordinate axis (Errico 1985), or fitting a two-dimensional plane to the data and then multiplying the values near the edges by a function that smoothly approaches zero at the boundary (Salvador et al. 1999). Denis et al. (2002) suggest the discrete cosine transform (DCT) offers the best approach for computing the spectra of aperiodic fields. We do not discuss the DCT here, but all of our formulas may be applied, with appropriate modification, to the DCT. Indeed, the application of the cosine transform to aperiodic data is conceptually equivalent to imposing symmetry boundary conditions at both edges of the domain, mirroring the existing data across one symmetry boundary, and applying a conventional Fourier transform on the expanded domain.

2. One-dimensional KE spectra

We begin by considering the properties of continuous fields. Neglecting the fluid density, the time- and space-averaged KE equals the KE spectral density $E(k)$ integrated over positive wavenumbers:

$$\left(\frac{\overline{\mathbf{u}\cdot\mathbf{u}}}{2}\right) = \frac{1}{L}\int_0^L \frac{\mathbf{u}\cdot\mathbf{u}}{2}\,dx = \int_0^\infty E(k)\,dk, \tag{3}$$

where $\mathbf{u} = (u, v)$ is the horizontal velocity vector, L is the length of the domain, and the spatial average is denoted by an overbar [Tennekes and Lumley (1972), their (8.1.5)]. The calculations for time averaging are obvious and will be ignored throughout the following.

Defining the continuous Fourier transform and its inverse as

$$\hat{u}(k) = \int_{-\infty}^{\infty} u(x)e^{2\pi ixk}\,dx,$$
$$u(x) = \int_{-\infty}^{\infty} \hat{u}(k)e^{-2\pi ixk}\,dk,$$

Parseval's theorem for continuous Fourier transforms is

$$\int_{-\infty}^{\infty} u^2\,dx = \int_{-\infty}^{\infty} \hat{u}(k)\hat{u}^*(k)\,dk.$$

Extending the definition of $u(x)$ to $[-\infty, \infty]$ by setting u to zero for all $x \notin [0, L]$ and using Parseval's theorem,

$$\overline{(u^2)} = \int_{-\infty}^{\infty} \frac{\hat{u}(k)\hat{u}^*(k)}{L}\,dk.$$

Since u is real, $\hat{u}(k) = \hat{u}^*(-k)$, and thus

$$\frac{1}{2}\int_{-\infty}^{\infty} \hat{u}(k)\hat{u}^*(k)\,dk = \int_0^\infty \hat{u}(k)\hat{u}^*(k)\,dk,$$

from which it follows that the KE spectral density in (3) may be written as

$$E(k) = \frac{\hat{u}(k)\hat{u}^*(k) + \hat{v}(k)\hat{v}^*(k)}{L}.$$

Note that the units of $\hat{u}(k)$ are meters squared per second, while those of $E(k)$ are meters cubed per second squared.

Our next goal is to find expressions for $E(k)$ appropriate for discrete versions of (3). Let (u_j, v_j) be the set of N gridpoint values of the x- and y-component velocities on the periodic mesh such that

$$x_j = (j-1)\Delta x, \quad j = 1, 2, \ldots, N, \tag{4}$$

where values at $x = 0$ match those at $x = L = N\Delta x$, and Δx is the grid spacing. FFTs are most efficient when N is a power of 2, or the product of powers of small prime numbers. We will therefore assume that N is even,

in which case the shortest wavelength on the mesh is exactly $2\Delta x$; the largest wavenumber is exactly $k_{\max} = \pi/\Delta x$, and the Fourier modes corresponding to wavenumbers $k_{\max}$ and $-k_{\max}$ are linearly dependent *on the discrete mesh*. As a consequence of this linear dependence, when N is even, the vector of Fourier coefficients $\hat{u}$ contains pairs of entries for positive and negative wavenumbers for every wavelength except those corresponding to $k = 0$ and $k_{\max}$. In our subsequent notation, we will assume that the coefficients of $k = 0$ and $k = k_{\max}$ are indexed in (2) when $m = 1$ and $m = N/2 + 1 \equiv N_m$, respectively.

Many FORTRAN routines for computing fast Fourier transforms, including FFTW and those in fftpack, are unnormalized and require the user to explicitly specify n_1 and n_2, in which case the simplest discrete expressions for $E(k)$ are obtained using $(n_1, n_2) = (1/N, 1)$. Since the case $(n_1, n_2) = (1/N, 1)$ is simplest, we consider it first; this is the opposite convention from that in Matlab and Python's numpy.fft.

a. Case $n_1 = 1/N$

If the $1/N$ normalization factor is attached to the forward transform ($n_1 = 1/N$), as derived in the appendix, the discrete Parseval relation becomes

$$\frac{1}{N}\sum_{j=1}^{N} u_j^2 = \sum_{m=1}^{N} \hat{u}_m \hat{u}_m^*, \tag{5}$$

implying that

$$\frac{1}{L}\sum_{j=1}^{N}\frac{u_j^2 + v_j^2}{2}\Delta x = \frac{1}{2}\sum_{m=1}^{N}(\hat{u}_m\hat{u}_m^* + \hat{v}_m\hat{v}_m^*) = \frac{1}{2\Delta k}\sum_{m=1}^{N}(\hat{u}_m\hat{u}_m^* + \hat{v}_m\hat{v}_m^*)\Delta k. \tag{6}$$

To identify an appropriate expression for Δk, note that the sum on the rhs of (6) represents a numerical quadrature such that

$$\sum_{m=1}^{N}(\hat{u}_m\hat{u}_m^* + \hat{v}_m\hat{v}_m^*)\Delta k \approx \int_{-k_{\max}}^{k_{\max}} \hat{u}(k)\hat{u}^*(k) + \hat{v}(k)\hat{v}^*(k)\, dk. \tag{7}$$

Temporarily assume $\hat{u}(k)\hat{u}^*(k) + \hat{v}(k)\hat{v}^*(k)$ and $\hat{u}_m\hat{u}_m^* + \hat{v}_m\hat{v}_m^*$ are one for all k, then $N\Delta k = 2k_{\max} = 2\pi/\Delta x$, and thus, $\Delta k = 2\pi/(N\Delta x) = 2\pi/L$. This is a natural choice in which Δk is simply the smallest nonzero value of k in the periodic domain.

Replacing the summation with twice the sum over positive wavenumbers (except for $k_{\max}$), and skipping wavenumber zero because we can assume the mean was removed before the spectral analysis, the discrete relation (6) may be expressed in a form directly comparable to (3) as

$$\frac{1}{L}\sum_{j=1}^{N}\frac{u_j^2 + v_j^2}{2}\Delta x = \sum_{m=2}^{N_m}\tilde{E}_m\Delta k, \tag{8}$$

where the discrete KE spectral density is

$$\tilde{E}_m = \frac{1}{(1+\delta_{m,N_m})}\frac{\hat{u}_m\hat{u}_m^* + \hat{v}_m\hat{v}_m^*}{\Delta k} = \frac{L}{2\pi(1+\delta_{m,N_m})}(\hat{u}_m\hat{u}_m^* + \hat{v}_m\hat{v}_m^*), \tag{9}$$

and δ_{m,N_m} is the Kronecker delta (the factor including this term prevents the spectral power from being erroneously doubled at $k = k_{\max}$). From (1), the units of $\hat{u}_m$ are meters per second, and therefore the units for $\tilde{E}_m$ in (9) are meters cubed per second squared, matching those for $E(k)$ in the continuous case.

b. Case $n_2 = 1/N$

Now suppose that following Matlab and Python's numpy.fft, the $1/N$ normalization factor is attached to the inverse transform ($n_2 = 1/N$). Then the discrete Parseval relation becomes

$$\sum_{j=1}^{N} u_j^2 = \frac{1}{N}\sum_{m=1}^{N}\hat{u}_m\hat{u}_m^*, \tag{10}$$

and the average KE in a domain of length L satisfies

$$\frac{1}{L}\sum_{j=1}^{N}\frac{u_j^2 + v_j^2}{2}\Delta x = \frac{\Delta x}{2NL}\sum_{m=1}^{N}(\hat{u}_m\hat{u}_m^* + \hat{v}_m\hat{v}_m^*). \tag{11}$$

The left side of (11) clearly approximates the left side of (3). The right side of (11) is again a sum over both positive and negative wavenumbers, which assuming zero amplitude at wavenumber zero, can be replaced by twice the sum over positive wavenumbers (except $k_{\max}$). Recalling that $\Delta k = 2\pi/L$, (11) may therefore be expressed as

$$\frac{1}{L}\sum_{j=1}^{N}\frac{u_j^2 + v_j^2}{2}\Delta x = \sum_{m=2}^{N_m}\breve{E}_m\Delta k, \tag{12}$$

where the discrete KE spectral density $\breve{E}_m$ for this alternative normalization is[1]

[1] The one-dimensional spectra computed in Durran and Weyn (2016) erroneously omitted a factor of $1/\pi$, which would have brought those results into closer agreement with observations.

$$\breve{E}_m = \frac{\Delta x}{2\pi N(1+\delta_{m,N_m})}(\hat{u}_m\hat{u}_m^* + \hat{v}_m\hat{v}_m^*). \quad (13)$$

Noting that

$$\breve{E}_m = \tilde{E}_m/N^2,$$

we conclude that the different choices for normalizing the discrete Fourier transform introduce large differences in the scaling of the KE spectral density.

3. Two-dimensional KE spectra

Let k_x and k_y be the dimensional wavenumbers in the x and y directions, and $\hat{u}(k_x, k_y)$ and $\hat{v}(k_x, k_y)$ be the two-dimensional Fourier transforms of the velocity field. Defining the total horizontal wavenumber as $k_h = (k_x^2 + k_y^2)^{1/2}$, the integral of the two-dimensional KE spectral density $E(k_h)$ again equals the integral of the KE averaged over the physical domain:

$$\left(\frac{\overline{\mathbf{u}\cdot\mathbf{u}}}{2}\right) = \int_0^\infty E(k_h)\,dk_h, \quad (14)$$

where $E(k_h)$ is the integral over all pairs (k_x, k_y) such that $k_h = (k_x^2 + k_y^2)^{1/2}$. To be specific, let $\mathbf{c}(\theta) = (k_h\cos\theta, k_h\sin\theta)$, then

$$E(k_h) = \frac{1}{2}\int_0^{2\pi}\{\hat{u}[\mathbf{c}(\theta)]\hat{u}^*[\mathbf{c}(\theta)] + \hat{v}[\mathbf{c}(\theta)]\hat{v}^*[\mathbf{c}(\theta)]\}k_h\,d\theta. \quad (15)$$

We wish to determine the discrete approximations to $E(k_h)$ appropriate for horizontal velocities $(u_{r,s}, v_{r,s})$ defined at grid points on the periodic mesh:

$$x_r = (r-1)\Delta x, \quad r = 1, 2, \ldots, N_x;$$
$$y_s = (s-1)\Delta y, \quad s = 1, 2, \ldots, N_y.$$

a. Case $n_1 = 1/N$

The appropriate discrete Parseval relation (5) generalizes to two dimensions in a straightforward way, such that

$$\frac{1}{N_xN_y}\sum_{r=1}^{N_x}\sum_{s=1}^{N_y}u_{r,s}^2 + v_{r,s}^2 = \sum_{l=1}^{N_x}\sum_{m=1}^{N_y}\hat{u}_{l,m}\hat{u}_{l,m}^* + \hat{v}_{l,m}\hat{v}_{l,m}^*. \quad (16)$$

Denoting the extent of the x and y domains as $L_x = N_x\Delta x$ and $L_y = N_y\Delta y$, and applying the same reasoning as in the 1D case, we obtain $\Delta k_x = 2\pi/L_x$ and $\Delta k_y = 2\pi/L_y$, allowing (16) to be written as

$$\frac{1}{L_xL_y}\sum_{r=1}^{N_x}\sum_{s=1}^{N_y}\frac{u_{r,s}^2 + v_{r,s}^2}{2}\Delta x\Delta y = \frac{L_xL_y}{8\pi^2}\sum_{l=1}^{N_x}\sum_{m=1}^{N_y}(\hat{u}_{l,m}\hat{u}_{l,m}^* + \hat{v}_{l,m}\hat{v}_{l,m}^*)\Delta k_x\Delta k_y. \quad (17)$$

The left-hand side of (17) approximates the left-hand side of (3), but the right-hand side needs to be replaced by a sum over the total wavenumber.

We discretize the 2D wavenumber in multiples of the maximum one-dimensional wavenumber, $\Delta k_h = \max(\Delta k_x, \Delta k_y)$, such that

$$k_p = p\Delta k_h, \quad p = 1, 2, \ldots, N_{\max},$$

where $N_{\max} = \lceil\sqrt{2}\max(N_x/2, N_y/2)\rceil$. Defining $R(p)$ as the set of wavenumber indices (l, m) satisfying

$$k_p - \Delta k_h/2 \le (k_{x_l}^2 + k_{y_m}^2)^{1/2} < k_p + \Delta k_h/2, \quad (18)$$

(17) may be written as

$$\frac{1}{L_xL_y}\sum_{r=1}^{N_x}\sum_{s=1}^{N_y}\frac{u_{r,s}^2 + v_{r,s}^2}{2}\Delta x\Delta y = \sum_{p=1}^{N_{\max}}\tilde{E}(k_p)\Delta k_h, \quad (19)$$

where

$$\tilde{E}(k_p) = \frac{L_xL_y\min(\Delta k_x, \Delta k_y)}{8\pi^2}\sum_{l,m\in R(p)}(\hat{u}_{l,m}\hat{u}_{l,m}^* + \hat{v}_{l,m}\hat{v}_{l,m}^*). \quad (20)$$

Note that the units of $\tilde{E}(k_p)$ are again meters cubed per second squared. This summation over total wavenumber is similar to that in Errico (1985), except that instead of choosing Δk_h to be $\min(\Delta k_x, \Delta k_y)$, we set it equal to the maximum to reduce the noise that would arise using the narrower spectral band.

For an isotropic grid with $\Delta x = \Delta y$ and $L_x = L_y \equiv L$, $\Delta k_x = \Delta k_y = \Delta k_h$,

$$\tilde{E}(k_p) = \frac{L}{4\pi}\sum_{l,m\in R(p)}(\hat{u}_{l,m}\hat{u}_{l,m}^* + \hat{v}_{l,m}\hat{v}_{l,m}^*). \quad (21)$$

We would only plot the spectrum $\tilde{E}(k_p)$ through wavenumber $k_h = N\Delta k_h/2$ because the data for higher wavenumbers are incomplete on the discrete mesh.

b. Case $n_2 = 1/N$

Parseval's relation becomes

$$\sum_{r=1}^{N_x}\sum_{s=1}^{N_y} u_{r,s}^2+v_{r,s}^2=\frac{1}{N_xN_y}\sum_{l=1}^{N_x}\sum_{m=1}^{N_y}\hat{u}_{l,m}\hat{u}_{l,m}^*+\hat{v}_{l,m}\hat{v}_{l,m}^*,$$

Using the notation introduced in section 3a, the average KE in the domain satisfies

$$\begin{aligned}&\frac{1}{L_xL_y}\sum_{r=1}^{N_x}\sum_{s=1}^{N_y}\frac{u_{r,s}^2+v_{r,s}^2}{2}\Delta x\Delta y\\&=\frac{\Delta x\Delta y}{2N_xN_yL_xL_y}\sum_{l=1}^{N_x}\sum_{m=1}^{N_y}\hat{u}_{l,m}\hat{u}_{l,m}^*+\hat{v}_{l,m}\hat{v}_{l,m}^*\\&=\frac{\Delta x\Delta y}{8\pi^2N_xN_y}\sum_{l=1}^{N_x}\sum_{m=1}^{N_y}(\hat{u}_{l,m}\hat{u}_{l,m}^*+\hat{v}_{l,m}\hat{v}_{l,m}^*)\Delta k_x\Delta k_y.\end{aligned}\tag{22}$$

Summing over annular rings in the $k_x - k_y$ plane, one obtains

$$\frac{1}{L_xL_y}\sum_{r=1}^{N_x}\sum_{s=1}^{N_y}\frac{u_{r,s}^2+v_{r,s}^2}{2}\Delta x\Delta y=\sum_{p=1}^{N_{\max}}\breve{E}(k_p)\Delta k_h,\tag{23}$$

where

$$\breve{E}(k_p)=\frac{\Delta x\Delta y\min(\Delta k_x,\Delta k_y)}{8\pi^2N_xN_y}\sum_{l,m\in R(p)}(\hat{u}_{l,m}\hat{u}_{l,m}^*+\hat{v}_{l,m}\hat{v}_{l,m}^*).\tag{24}$$

For an isotropic square grid,

$$\breve{E}(k_p)=\frac{L}{4\pi N^4}\sum_{l,m\in R(p)}(\hat{u}_{l,m}\hat{u}_{l,m}^*+\hat{v}_{l,m}\hat{v}_{l,m}^*),\tag{25}$$

implying that in the case of two-dimensional spectra,

$$\breve{E}(k_p)=\tilde{E}(k_p)/N^4.$$

4. Reducing discretization noise in 2D spectra

The summation over annular rings in the $k_x - k_y$ plane computed, for example in (20), introduces *systematic* noise in 2D spectra because the number [or count $C(p)$] of wavenumber pairs in set $R(p)$ does not increase smoothly with k_p. As noted in Tanguay et al. (1995), one can compensate for this systematic noise by multiplying the KE spectral density at each discrete k_p by

$$\frac{2\pi k_p}{\Delta k_\perp}\frac{1}{C(p)},\tag{26}$$

where $\Delta k_\perp = \min(\Delta k_x, \Delta k_y)$. Given that $\Delta k_h = \max(\Delta k_x, \Delta k_y)$ is the discrete grid interval along the radial direction, $\Delta k_\perp$ may be interpreted as the effective grid interval around the circumference of the annulus (18) in the $k_x - k_y$ plane. Thus, (26) represents the ratio of the number of wavenumber pairs that would be expected around a ring of radius k_p divided by the actual number of pairs falling in the annulus (18).

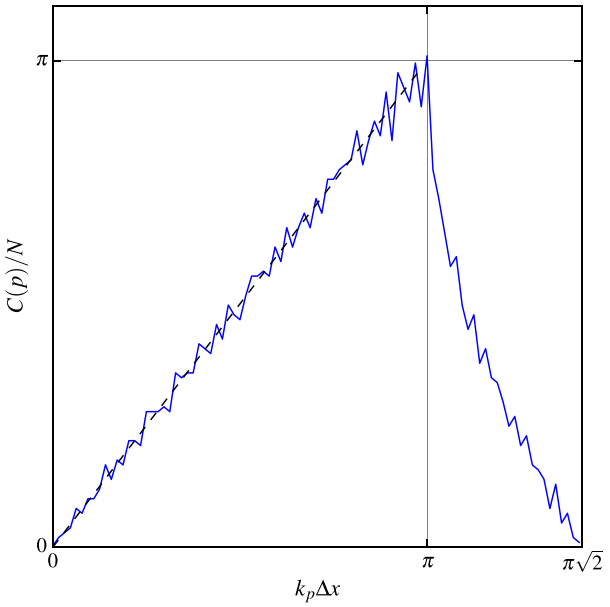

FIG. 1. Normalized number of wavenumber pairs within each total wavenumber bin $C(p)/N$ plotted as a function of $k_p\Delta x$, for a square domain with 128 grid points along each coordinate (blue). The black dashed line shows the expected number of wavenumber pairs for each $k_p\Delta x$ over the interval $0 \le k_p\Delta x \le \pi$.

A few previous studies also mention the use of factors similar to (26) to reduce noise (Bartello 1995; Waite 2016), but it is unclear how commonly this type of compensation has been employed. In particular, it is not discussed in Errico (1985), which gives a detailed algorithm for the computation of two-dimensional spectra that has been frequently cited. In the remainder of this section, we document the significant improvements that can be achieved using such compensation and suggest a modest improvement to the formulation in (26). Note that the discrete Parseval relation no longer holds after multiplying the spectral densities by (26).

In an isotropic square domain, $\Delta k_\perp = 2\pi/L$ and the factor in (26) may be alternatively expressed $Lk_p/C(p)$. Figure 1 shows $Lk_p = Nk_p\Delta x$ plotted as a function of $k_p\Delta x$ as the black dashed line terminating at the value of $k_p\Delta x$ corresponding to a $2\Delta x$ wave. Also shown in Fig. 1 is $C(p)/N$ for the case $N = 128$, which roughly follows the line $Nk_p\Delta x$ over the interval $[0, \pi]$ and then quickly falls to one at $k_p\Delta x = \sqrt{2}\pi$ because of the rapid increase in the number of missing (k_x, k_y) pairs at wavelengths shorter than $2\Delta x$. The fluctuations of $C(p)/N$ about the line $Nk_p\Delta x$ are not random; they leave an imprint on

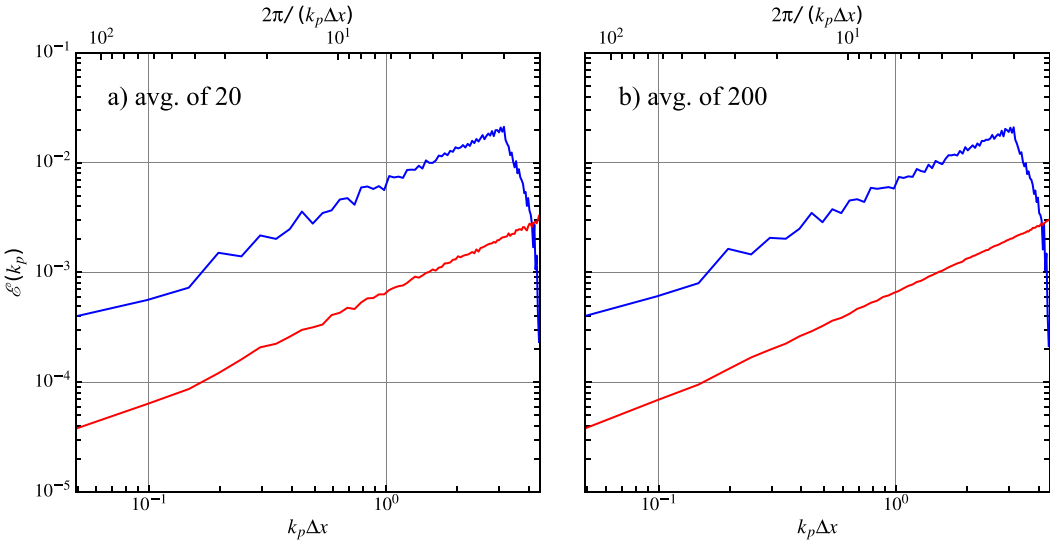

FIG. 2. Two-dimensional energy spectral density for random white noise in a 128 × 128 square domain averaged over (a) 20 samples and (b) 200 samples. The blue line is the result of the standard summation over annular rings in the wavenumber domain; the red line shows the result after multiplication by the noise compensating factor in (28), shifted down by a factor of 10 for clarity. The top axis is labeled in units of wavelength divided by Δx.

two-dimensional spectra that are computed using the summation procedure in (20), and they can be removed through multiplication by the factor (26).

The distribution of the data from two-dimensional FFTs is very nonlinear in spectral space, with just a few widely spaced points corresponding to the smallest wavenumbers, and many closely spaced points at larger wavenumbers. To improve the performance of the preceding noise compensation at very small wavenumbers, where the numerical resolution as a function of k_h is very coarse, it is helpful to replace k_p in (26) by the average k_h for all wavenumber pairs in $R(p)$, which will be denoted by $\overline{k}_p$. Then the noise-compensated spectral density corresponding to (20) would become

$$\tilde{E}_c(k_p) = \frac{L_x L_y \overline{k}_p}{4\pi C(p)} \sum_{l,m\in R(p)} (\hat{u}_{l,m}\hat{u}^*_{l,m} + \hat{v}_{l,m}\hat{v}^*_{l,m}). \quad (27)$$

The effectiveness of this noise removal procedure is illustrated in two examples. First consider a randomly distributed scalar variable with zero mean defined on a 128×128 gridpoint square domain. The energy spectral density $\mathscr{E}(k_p)$, computed with and without multiplication by

$$\frac{2\pi\overline{k}_p}{\Delta k_\perp}\frac{1}{C(p)}, \quad (28)$$

and averaged over 20 or 200 samples, is plotted as a function of $k_p\Delta x$ in Fig. 2. As expected for two-dimensional white noise, the energy spectral density increases roughly linearly with wavenumber over the interval $[0, \pi]$. Whether averaged over 20 or 200 samples, the uncompensated spectra (blue lines) look quite similar, and show significant noise. On the other hand, the energy spectral densities compensated through multiplication by (28) look much smoother and the remaining noise is greatly reduced as the sample size is increased from 20 to 200. Multiplication by (28) also corrects these spectra for wavelengths shorter than $2\Delta x$ (i.e., for wavenumbers in the range $\pi \le k_p\Delta x \le \sqrt{2}\pi$), but one should not attach confidence to results for such wavelengths in practice.

Figure 3 shows the mean horizontal KE spectral density in a 20-member ensemble of numerical simulations of idealized squall lines, initialized with slightly different humidity fields, conducted using a 512 × 512 periodic domain. In addition to the ensemble average, the spectra were averaged over the vertical layer $10 \le z \le 12$ km (Weyn and Durran 2017, their Fig. 6e). The blue curve shows the spectra computed using Python's numpy.fft and (25); the red curve shows the same result, shifted down by a factor of 10 for visibility, after compensating for the discretization noise by multiplying by the factor (28), in which case the compensated KE spectral density is

$$\breve{E}_c(k_p) = \frac{L^2 \overline{k}_p}{4\pi N^4 C(p)} \sum_{l,m\in R(p)} (\hat{u}_{l,m}\hat{u}^*_{l,m} + \hat{v}_{l,m}\hat{v}^*_{l,m}). \quad (29)$$

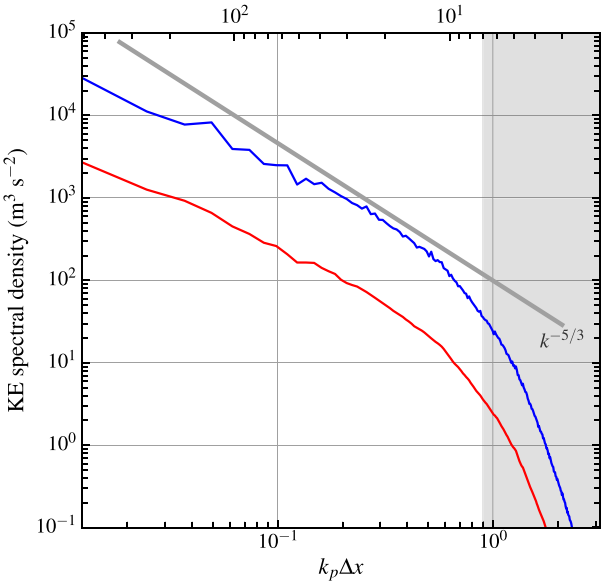

FIG. 3. Two-dimensional KE spectral density from idealized squall-line simulations. The blue line is the result of the standard summation over annular rings in the wavenumber domain. The red line shows the result after multiplication by the noise-compensating factor (28) and is shifted down by a factor of 10 for better visibility. The portion of the spectrum corresponding to wavelengths shorter than $7\Delta x$ is shaded. The thick gray line follows a $k^{-5/3}$ slope.

Despite the vertical and ensemble averaging, the uncompensated KE spectrum remains noisy. The compensated KE spectrum, on the other hand, is quite smooth.

5. Relationship between one- and two-dimensional power-law spectra

If the two-dimensional KE spectral density of a nondivergent isotropic flow obeys the power-law $E(k_h) = \alpha_2 k_h^\beta$, for $\beta < 0$, one-dimensional KE spectral densities obey the same power law, with a different constant of proportionality [i.e., $E_1(k_x) = \alpha_1 k_x^\beta$]. Most atmospheric observations are analyzed along lines (e.g., along an aircraft flight track). If one wishes to compare two-dimensional KE spectra from a model with observations of one-dimensional spectra, one should correct for the difference between α_1 and α_2. Leith (1971) showed that

$$E_1(k_x) = \frac{2}{\pi}\int_{k_x}^{\infty} \frac{E(k_h)}{(k_h^2 - k_x^2)^{1/2}}\, dk_h, \tag{30}$$

or letting $s = k_h/k_x$, $ds = dk_h/k_x$, and substituting for $E(k_h)$,

$$E_1(k_x) = \frac{2\alpha_2 k_x^\beta}{\pi}\int_1^{\infty} \frac{s^\beta}{(s^2-1)^{1/2}}\, ds. \tag{31}$$

Leith (1971) noted that for $\beta = -3$, $\alpha_1 = \alpha_2/2$, but did not consider other values of β. For $\beta < 0$ the integral in (31) converges, giving

$$E_1(k_x) = \frac{\Gamma\left(-\frac{\beta}{2}\right)}{\sqrt{\pi}\,\Gamma\left(\frac{1}{2}-\frac{\beta}{2}\right)} E(k_x). \tag{32}$$

If $\beta = -1$, $\alpha_1 = \alpha_2$, and in the important case $\beta = -5/3$, $\alpha_1 \approx 0.713\alpha_2$ (Lindborg 1999; Durran and Gingrich 2014).

The analytic result (32) does not exactly hold for spectra computed from gridded data due to numerical errors. To assess the nature of these errors, nondivergent flows were computed from a streamfunction of the following form:

$$\hat{\psi}(k_x, k_y) = e^{i\phi}(k_x^2 + k_y^2)^{(\beta-3)/2},$$

where (k_x, k_y) are the wavenumber pairs for the discrete data, $\phi \in [-\pi, \pi]$ is a random phase, and the condition $\hat{\psi}(k_x, k_y) = \hat{\psi}^*(-k_x, -k_y)$ is enforced to ensure $\psi(x, y)$ is real. According to (15), the horizontal velocities

$$\hat{u} = -ik_y\hat{\psi}, \quad \hat{v} = ik_x\hat{\psi},$$

will yield a KE spectral density for which $E(k_h) \propto k_h^\beta$.

One- and two-dimensional KE spectral densities, computed from single realizations of this idealized velocity field on a 512×512 isotropic mesh, are plotted in Fig. 4 for the cases $\beta = -3$, $-5/3$, and -1. The 1D spectral densities were computed from (13) using one-dimensional transforms along the x coordinate at each of the 512 y-coordinate values, and then averaged over y. The 2D spectral densities were computed from (29) and scaled by the factor $\alpha_1(\beta)/\alpha_2(\beta)$.

As evident in Fig. 4, the α_1/α_2 scaling does a good job of mapping the 2D spectra exactly onto the corresponding 1D curve. Nevertheless, the 2D spectra fall slightly below the 1D spectra and the expected k_p^β line at very small wavenumbers. This is due to the previously discussed issue of coarse numerical resolution at very small wavenumbers. In contrast, at very large wavenumbers, it is the 1D spectra that fall below the k_p^β line, and the discrepancy becomes much larger as β increases from -3 to -1. This difference arises because, instead of extending to infinity, the numerical equivalent of the integral in (30) is effectively truncated at $k_x = k_{\max} = \pi/\Delta x$. When $\beta = -3$, the contribution from the unresolved high wavenumbers, and the high-wavenumber difference between the 1D and 2D spectra is much smaller than when $\beta = -1$. Although the high-wavenumber falloff in the amplitude of the 1D spectra in

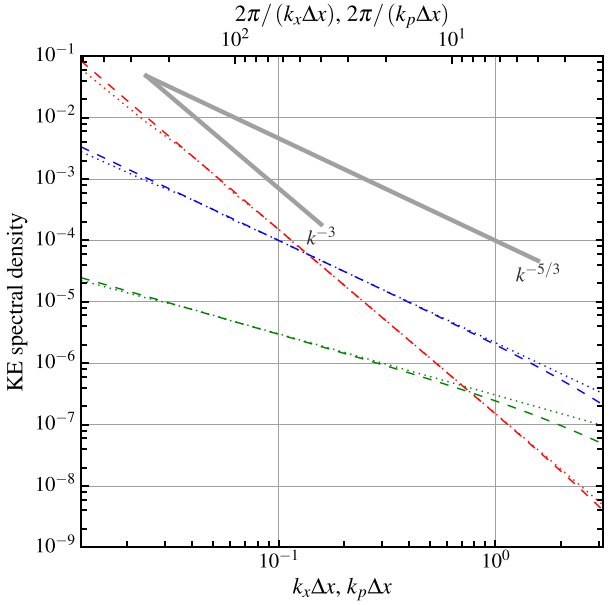

FIG. 4. One-dimensional (dashed) and two-dimensional (dotted) KE spectral densities plotted as a function of $k_x\Delta x$ and $k_p\Delta x$, respectively, for nondivergent velocity fields analytically specified on an isotropic 512×512 mesh to follow k_h^{-3} (red), $k_h^{-5/3}$ (blue), and k_h^{-1} (green) spectral slopes. The blue lines are shifted up by a factor of 10 for better visibility. The top axis is labeled in units of wavelength divided by Δx.

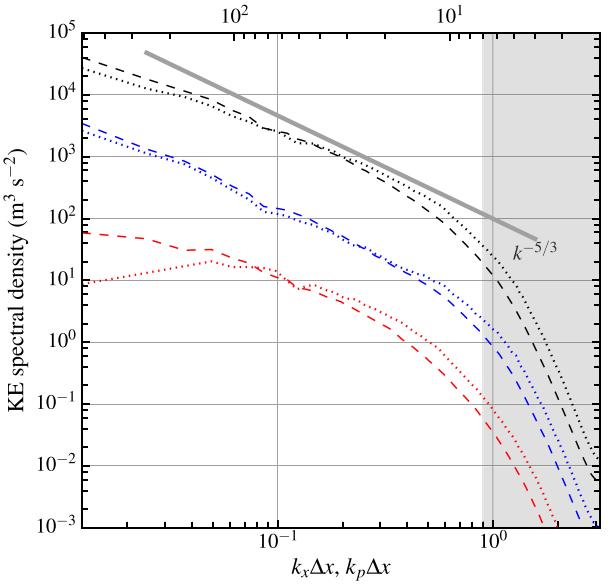

FIG. 5. One-dimensional (dashed) and two-dimensional (dotted) KE spectral densities plotted as a function of $k_x\Delta x$ and $k_p\Delta x$, respectively, for the ensemble of squall-line simulations shown in Fig. 3. Black curves are the full KE; blue curves are the KE of the divergent component, reduced by a factor of 10 for visibility; and red curves are the KE of the rotational component, reduced by a second factor of 10. The top axis is wavelength in units of Δx.

Fig. 4 is much weaker than that caused by numerical dissipation in typical numerical simulations (as illustrated, e.g., in Fig. 3), it is worth noting that a modest falloff should be expected at high wavenumbers even in the absence of dissipation.

The derivation of (32) assumes nondivergent two-dimensional isotropic flow, but the relationship between α_1 and α_2 can also hold in at least some completely divergent, anisotropic flows. This good behavior is illustrated in Fig. 5, which compares 1D and 2D spectra from the ensemble of squall-line simulations already considered in Fig. 3. The total flow is decomposed into divergent and rotational components as described in Weyn and Durran (2017), who also noted that the divergent component closely follows a $k_h^{-5/3}$ spectrum. Scaling the 2D divergent KE spectrum such that $\alpha_1 = 0.713\alpha_2$ maps the 1D and 2D spectra onto almost the same curve. In contrast, the rotational KE does not follow a power law as closely (i.e., it does not plot as a straight line), and the slopes of the 1D and 2D spectra are not as similar as those for the divergent winds.

6. Conclusions

In this paper we have considered the computation of horizontal KE spectra as our primary example, but equivalent expressions apply when computing the spectrum of any scalar variable. The correct dimensional scaling of the energy density spectra depends strongly on the normalization used in the discrete Fourier transform routines. The "traditional" choice of $n_1 = 1/N$, $n_2 = 1$ in (1) and (2) leads to the relatively intuitive expressions (9) and (20) for the one- and two-dimensional KE spectral density, respectively. Matlab and Python's numpy.fft routines use the alternative normalization $(n_1, n_2) = (1, 1/N)$ and as a consequence, the corresponding KE spectral densities (13) and (24) differ for those computed with the traditional choice by factors of N^2 in the one-dimensional case and N^4 in a square two-dimensional domain.

Two-dimensional spectra computed by summing over wavenumber pairs (k_x, k_y) in annular bins exhibit systematic noise owing to the nonsmooth increase in the count of wavenumber pairs in each bin as the total wavenumber k_h increases. One can compensate for this noise by multiplying the energy spectral density at each discrete k_h by the factor (28). If the underlying data are sufficiently smoothed by ensemble, temporal, or spatial averaging, the improvement produced by this procedure can be pronounced.

If the two-dimensional KE spectral density is proportional to k_h^β and $\beta < 0$, one-dimensional spectral densities for the same flow will follow the same k_h^β power

law, but with a different constant of proportionality given by (32). This theoretical result is formally derived for isotropic nondivergent flows, but was found to also work well for a divergent anisotropic example. In the discrete case, the truncation of the data at some maximum wavenumber leads to a modest decrease in the one-dimensional spectral density relative to the corresponding two-dimensional value at high wavenumbers. Nevertheless, when $\beta = -5/3$ the falloff at high wavenumbers is much weaker than that produced by numerical dissipation in typical atmospheric models.

Acknowledgments. The paper was improved through very helpful discussions with Mike Waite and Jim Riley, and also by the comments of two anonymous reviewers. This research is funded by NSF Grant AGS-1545927 and Grant N000141410287 from the Office of Naval Research (ONR). JAW was supported by a National Defense Science and Engineering Graduate (NDSEG) Fellowship.

APPENDIX

The Discrete Parseval Relation

A typical derivation of the discrete Parseval theorem is provided here to help the reader appreciate the impact of different choices for n_1 and n_2. From (2) and our previously defined notation,

$$u_j = n_2 \sum_{m=1}^{N} \hat{u}_m e^{2\pi i(m-1)(j-1)/N}. \tag{A1}$$

Allowing for complex values of u_j, which is the most general case (and required as part of two-dimensional Fourier transforms),

$$\begin{aligned} |u_j|^2 &= |u_j u_j^*| \\ &= n_2^2 \left(\sum_{m=1}^{N} \hat{u}_m e^{2\pi i(m-1)(j-1)/N} \right) \left(\sum_{m'=1}^{N} \hat{u}_{m'}^* e^{-2\pi i(m'-1)(j-1)/N} \right) \\ &= n_2^2 \sum_{m=1}^{N} \hat{u}_m \left(\sum_{m'=1}^{N} \hat{u}_{m'}^* e^{2\pi i(m-m')(j-1)/N} \right). \end{aligned}$$

Thus,

$$\sum_{j=1}^{N} |u_j|^2 = n_2^2 \sum_{m=1}^{N} \sum_{m'=1}^{N} \hat{u}_m \hat{u}_{m'}^* \sum_{j=1}^{N} (e^{2\pi i(m-m')/N})^{(j-1)}. \tag{A2}$$

Using the finite sum of a geometric series

$$1 + q + q^2 + \cdots + q^N = \frac{1 - q^{N+1}}{1 - q},$$

for $m \neq m'$ the last summation in (A2) becomes

$$\sum_{j=1}^{N} (e^{2\pi i(m-m')/N})^{(j-1)} = \frac{1 - e^{2\pi i(m-m')}}{1 - e^{2\pi i(m-m')/N}} = 0.$$

If $m = m'$, the last summation in (A2) is simply N, and therefore (A2) reduces to

$$\sum_{j=1}^{N} |u_j|^2 = N n_2^2 \sum_{m=1}^{N} \hat{u}_m \hat{u}_m^*, \tag{A3}$$

showing that the choice $n_2 = 1$ yields (5), whereas $n_2 = 1/N$ gives (10).

REFERENCES

Bartello, P., 1995: Geostrophic adjustment and inverse cascades in rotating stratified turbulence. *J. Atmos. Sci.*, **52**, 4410–4428, doi:10.1175/1520-0469(1995)052<4410:GAAICI>2.0.CO;2.

Cho, J. Y. N., and Coauthors, 1999: Horizontal wavenumber spectra of winds, temperature, and trace gases during the Pacific Exploratory Missions: 1. Climatology. *J. Geophys. Res.*, **104**, 5697–5716, doi:10.1029/98JD01825.

Cooley, J., P. Lewis, and P. Welch, 1970: The fast Fourier transform algorithm: Programming considerations in the calculation of sine, cosine and Laplace transforms. *J. Sound Vibrat.*, **12**, 315–337, doi:10.1016/0022-460X(70)90075-1.

Denis, B., J. Coté, and R. Laprise, 2002: Spectral decomposition of two-dimensional atmospheric fields on limited-area domains using the discrete cosine transform (DCT). *Mon. Wea. Rev.*, **130**, 1812–1829, doi:10.1175/1520-0493(2002)130<1812:SDOTDA>2.0.CO;2.

Durran, D. R., 2010: *Numerical Methods for Fluid Dynamics: With Applications to Geophysics.* 2nd ed. Springer-Verlag, 516 pp.

——, and M. Gingrich, 2014: Atmospheric predictability: Why butterflies are not important. *J. Atmos. Sci.*, **71**, 2476–2488, doi:10.1175/JAS-D-14-0007.1.

——, and J. Weyn, 2016: Thunderstorms do not get butterflies. *Bull. Amer. Meteor. Soc.*, **97**, 237–243, doi:10.1175/BAMS-D-15-00070.1.

Errico, R., 1985: Spectra computed from a limited area grid. *Mon. Wea. Rev.*, **113**, 1554–1562, doi:10.1175/1520-0493(1985)113<1554:SCFALA>2.0.CO;2.

Hamilton, K., Y. O. Takahashi, and W. Ohfuchi, 2008: Mesoscale spectrum of atmospheric motions investigated in a very fine resolution global general circulation model. *J. Geophys. Res.*, **113**, D18110, doi:10.1029/2008JD009785.

Leith, C., 1971: Atmospheric predictability and two-dimensional turbulence. *J. Atmos. Sci.*, **28**, 145–161, doi:10.1175/1520-0469(1971)028<0145:APATDT>2.0.CO;2.

Lindborg, E., 1999: Can the atmospheric kinetic energy spectrum be explained by two-dimensional turbulence? *J. Fluid Mech.*, **388**, 259–288, doi:10.1017/S0022112099004851.

Nastrom, G., and K. Gage, 1985: A climatology of atmospheric wavenumber spectra of wind and temperature observed by commercial aircraft. *J. Atmos. Sci.*, **42**, 950–960, doi:10.1175/1520-0469(1985)042<0950:ACOAWS>2.0.CO;2.

Salvador, R., J. Calbó, and M. M. Millán, 1999: Horizontal grid size selection and its influence on mesoscale model simulations. *J. Appl. Meteor.*, **38**, 1311–1329, doi:10.1175/1520-0450(1999)038<1311:HGSSAI>2.0.CO;2.

Skamarock, W. C., 2004: Evaluating mesoscale NWP models using kinetic energy spectra. *Mon. Wea. Rev.*, **132**, 3019–3024, doi:10.1175/MWR2830.1.

Tanguay, M., P. Bartello, and P. Gauthier, 1995: Four-dimensional data assimilation with a wide range of scales. *Tellus*, **47A**, 974–997, doi:10.3402/tellusa.v47i5.11967.

Tennekes, H., and J. Lumley, 1972: *A First Course in Turbulence.* MIT Press, 300 pp.

Waite, M. L., 2016: Dependence of model energy spectra on vertical resolution. *Mon. Wea. Rev.*, **144**, 1407–1421, doi:10.1175/MWR-D-15-0316.1.

Weyn, J. A., and D. R. Durran, 2017: The dependence of the predictability of mesoscale convective systems on the horizontal scale and amplitude of initial errors in idealized simulations. *J. Atmos. Sci.*, **74**, 2191–2210, doi:10.1175/JAS-D-17-0006.1.